BBA - General Subjects xxx (xxxx) xxx–xxx

Contents lists available at ScienceDirect

BBA - General Subjects

journal homepage: www.elsevier.com/locate/bbagen

# Direct visualization of avian influenza H5N1 hemagglutinin precursor and its conformational change by high-speed atomic force microscopy

Kee Siang Lim[a], Mahmoud Shaaban Mohamed[b], Hanbo Wang[c], Hartono[c], Masaharu Hazawa[a,b,c], Akiko Kobayashi[a], Dominic Chih-Cheng Voon[d], Noriyuki Kodera[a], Toshio Ando[a], Richard W. Wong[a,b,c,*]

[a] WPI Nano Life Science Institute (WPI-NanoLSI), Kanazawa University, Kakuma-machi, Kanazawa, Japan.
[b] Cell-Bionomics Research Unit, Innovative Integrated Bio-Research Core, Institute for Frontier Science Initiative, Kanazawa University, Kanazawa, Japan
[c] Faculty of Natural System, Institute of Natural Science and Technology, Kanazawa University, Kanazawa, Japan
[d] Cancer Model Research Innovative Unit, Institute for Frontier Science Initiative, Kanazawa University, Kanazawa, Japan

ARTICLE INFO

*Keywords:*
Influenza A
Hemagglutinin
HA0 trimer
Conformational dynamic
High-speed atomic force microscopy

ABSTRACT

*Background:* Hemagglutinin (HA) of influenza A is one of the key virulence factors that mediates the release of viral components in host cells. HA is initially synthesized as a trimeric precursor (HA0) and then it is cleaved by proteases to become a functional HA. Low pH induces irreversible conformational changes in both HA0 and HA but only HA is fusion compatible. Here, we used high-speed atomic force microscopy (HS-AFM) to record conformational changes in HA0 trimers (H5N1) from neutral to acidic conditions at a millisecond scale.

*Methods:* Purified HA0 protein was diluted with either neutral Tris-HCl (pH 7.4) or acetic acid-titrated Tris-HCl (pH 5.0) and then loaded onto bare mica. Neutral or acidic Tris-HCl was used as the scanning buffer. HS-AFM movies were recorded and processed using Image J software.

*Results:* The conformation of $HA0_{neutral}$ visualized using HS-AFM was comparable to the HA trimer structures depicted in the PDB data and the AFM simulator. HA0 underwent rapid conformational changes under low pH condition. The circularity and area of $HA0_{acid}$ were significantly higher than in $HA0_{neutral}$. In contrast, the height of $HA0_{acid}$ was significantly lower than in $HA0_{neutral.}$

*Conclusions:* We have captured real-time images of the native HA0 trimer structure under physiological conditions using HS-AFM. By analyzing the images, we confirm that HA0 trimer is sensitive to acidic conditions.

*General significance:* The dynamic nature of the HA structure, particularly in the host endosome, is essential for H5N1 infectivity. Understanding this acidic behavior is imperative for designing therapeutic strategies against H5N1. This article reports a sophisticated new tool for studying the spatiotemporal dynamics of the HA precursor protein.

## 1. Introduction

The *Orthomyxoviridae* family consists of three members, namely influenza A, influenza B, and influenza C [1]. Viral glycoprotein hemagglutinin (HA) and viral glycoprotein enzyme neuraminidase (NA) are found in influenza A and influenza B viruses. By contrast, influenza C expresses the membrane HA–esterase fusion glycoprotein, whose function is a combination of HA and NA [2]. Both HA and NA are used for subtype classification of influenza A, but this is not applicable to influenza B. Among these three members, influenza A has caused several devastating pandemics in human history. For instance, the H1N1 pandemic in 1918 resulted in an estimated 50–100 million deaths worldwide [3]. Unlike influenza B and C, gene reassortment in influenza A of the HA and NA combination produces a new virus subtype. As a result, the newly emergent virus can infect new hosts, including humans, creating therapeutic challenges due to the lack of appropriate antibodies. For example, the flu pandemic in 1968 was caused by H3N2, a virus derived from H2N2 virus (flu pandemic in 1957) after multiple gene reassortment events [4].

HA is synthesized and post-translationally modified in the endoplasmic reticulum (ER) followed by trimerization to become the HA precursor known as HA0 [5]. Each monomer comprises of two domains,

* Corresponding author at: WPI Nano Life Science Institute (WPI-NanoLSI), Unit Leader in Cell-Bionomics Research Unit, Institute for Frontier Science Initiative, Kanazawa University, Kakuma-machi, Kanazawa 920-1192, Japan.
*E-mail address:* rwong@staff.kanazawa-u.ac.jp (R.W. Wong).

https://doi.org/10.1016/j.bbagen.2019.02.015
Received 7 December 2018; Received in revised form 19 February 2019; Accepted 26 February 2019

designated HA1 and HA2, which are linked by disulfide bonds. HA1 contains the globular receptor binding region, vestigial esterase, and the fusion (F′) subdomains [6]. Whereas, HA2, the domain that possesses a fusion peptide needed for membrane fusion, stabilizes HA on the viral envelope via its transmembrane domain [6]. To ensure infectivity of influenza A, HA0 needs to be cleaved by proteases to free the HA1 and HA2 domains. The properties of the HA cleavage site determine whether cleavage occurs intracellularly (polybasic cleavage site) [6] or extracellularly (monobasic cleavage site) [7,8]. The presence of a polybasic cleavage site confers high pathogenicity in influenza A virus as the virus causes systemic dissemination in the host. Whereas, the presence of a monobasic cleavage site limits viral distribution to specific sites such as the respiratory tract [6]. The receptor binding site of HA binds to sialic acid expressed on the cellular surface of host cells. The host specificity of influenza A depends on the compatibility between HA and sialic acids. For example, avian influenza A binds to α (2,3)-linked sialic acid, whereas human influenza A binds to α (2,6)-linked sialic acid [9–12]. Mutation of the receptor binding site allows cross species infection with the same influenza virus. Upon binding to host cells, viral entry occurs through host endocytosis. Cleavage of HA0 produces a metastable HA in which HA2 undergoes irreversible conformational changes in the acidic endosomal environment. This change allows the fusion peptide to attach to the endosomal membrane to initiate membrane fusion. Membrane fusion is a crucial process as it releases viral components into host cells.

HA is a well-characterized viral membrane glycoprotein. Comprehensive structural investigations of HA have been performed using various sophisticated tools such as X-ray crystallography [7,13], cryo-electron microscopy (cryo-EM) [14–16], and nuclear magnetic resonant (NMR) ([17,18]. Understanding the HA structure, particularly its dynamic nature, is essential for determining effective therapeutic strategies against influenza A. Both HA0 and HA display dynamic structures under specific conditions. Boulay and coworkers [19] reported that HA0 of H3N2 underwent irreversible conformation alterations at pH values < 6. Acidification of HA0 changed its susceptibility to trypsin digestion and hence indicated conformational changes. However, the acidic conformation of HA0 was fusogenic incompetent. Bullough and colleagues used X-ray crystallography to show that HA0 was stable, whereas HA was metastable in low pH environments [20]. Dynamic conformational changes in the HA2 domain were much more complex. Using the single molecule fluorescence resonance energy transfer (smFRET) imaging technique, Das and colleagues [21] reported that structural changes in the HA2 domain of H5N1 were reversible. Several external factors such as receptor–ligand interactions, a low pH environment, and the presence of the host endosomal membrane, determine the HA2 conformation. The team reported the HA2 structures in various states: pre-fusion, intermediate (I and II), extended intermediate, and post-fusion. Such complex dynamic behavior prevents early inactivation of HA and thus ensures successive membrane fusion.

The aforementioned technical approaches generate robust, good quality results for characterization of the HA structure. However, images obtained using these approaches are static and thus limit researchers when studying dynamic structural changes and dynamic interactions of biomolecules. Atomic force microscopy (AFM) has gained popularity as it captures biomolecules in their physiological condition. AFM has been used for identifying specific molecules and determining their location in a complex [22,23], for measuring molecular bonding forces [24,25], the surface elasticity of biomolecules [26,27], and the osmotic pressure of living cells [28]. Barinov and colleagues used high resolution AFM to study the oligomeric structure of the HA of several subtypes of influenza A and their conformational changes due to pH and binding effects (ligands, antibody, or DNA aptamer) [29]. Conventional AFM has a slow scanning speed and therefore is not suitable for imaging biomolecules with highly dynamic behavior. However, recent technical improvements have resulted in AFM with high scanning speed, known as high-speed AFM (HS-AFM). HS-AFM can be used to capture real-time structural changes in proteins and dynamic interactions of proteins without damaging the delicate protein samples at nanoscale [27,30]. This high speed and minimally invasive method has successfully revealed several important biological activities such as the dynamic motion of myosin on actin [31], the cleavage of DNA by Cas9 protein [32], the interaction of two clock proteins KaiA and KaiC that is required for regulating circadian rhythm [33], and biological activity in the nuclear pore complex [34]. Protein structures recorded using HS-AFM are comparable to the structures observed using other methods, for example, cryo-EM.

HS-AFM is an exceptional tool for the examination of protein dynamics in native environments, in physiological buffer, and at ambient temperature and pressure, with ~1 nm lateral, ~0.1 nm vertical, and ~100 ms temporal resolution [34,35]. In this study, we used HS-AFM to directly visualize the recombinant HA0 trimer of H5N1 protein. The HA0 structure determined in this study was comparable to the structures derived from both the PDB file and the AFM-simulated HA0 image. We also investigated the conformational differences in HA0 between neutral ($HA0_{neutral}$) and acidic ($HA0_{acid}$) conditions. Our results indicated that an acidic environment (pH 5.0) induces structural changes in the HA0 trimer. In summary, HS-AFM is feasible for observing dynamic changes of HA and has the potential to capture the highly dynamic HA2 domain that is crucial for viral infectivity in the near future.

## 2. Materials and methods

### 2.1. Sample preparation

Recombinant HA of influenza A subtype H5N1 (A/Hong Kong/483/9711689-V08H) was purchased from Sino Biological Inc. (Beijing, China). The recombinant HA is a trimeric protein with uncleaved HA1 and HA2 and is thus considered as HA0 trimer. HA0 trimer was reconstituted in milliQ water at 0.2 mg/ml and was then further diluted 100-fold with ultrapure 50 mM Tris-HCl purchased from Thermo Scientific (pH 7.4) for HS-AFM scanning. For visualization of $HA0_{acid}$, HA0 trimer was diluted 100-fold with acetic acid (Nacalai Tesque)-titrated 50 mM Tris-HCl (pH 5.0).

### 2.2. Cantilever preparation

Cantilever model BL-AC10DS-A2 (Olympus) with a spring constant (k) of 0.1 N/m and a resonance frequency (f) of 0 .6MHz in water (1.5 MHz in air) was used as a scanning probe to visualize HA0. The dimensions of the cantilever were as follows: 9 μm (length), 2 μm (width), and 0.13 μm (thickness). To improve resolution, a sharp carbon tip with a lower apex radius was grown on the existing tip of the cantilever by electron-beam deposition using a field emission scanning electron microscope (ELS-7500, Elionix). Electron-beam deposition was performed at 30 kV accelerating voltage and two minutes of irradiation. The cantilever was cleaned by UV/O3 and then by piranha solution (mixture of sulfuric acid and hydrogen peroxide).

### 2.3. HS-AFM visualization

A laboratory-built tapping mode (2 nm free amplitude, ~2.2 MHz) high-speed atomic force microscope (HS-AFM) [34] equipped with a narrow-range scanner was used to visualize the HA0 trimer. The scanner was mounted with a glass stage coated with ultra-thin and ultra-flat muscovite mica layers, which function as substrate for HA0 trimer adsorption, and 3 μl of diluted HA0 sample was dropped onto the bare mica layer and incubated for 5 min. Then, the mica was washed with ultrapure 50 mM Tris-HCl buffer (pH 7.4) and HS-AFM scanning was performed. Ultrapure 50 mM Tris-HCl buffer (pH 7.4) was used as the scanning buffer. To visualize $HA0_{acid}$, acidic 50 mM Tris-HCl buffer (pH 5.0) was used to wash the mica and also as the scanning buffer.

During scanning, the laser beam, with a wavelength of 670 nm, was focused onto the cantilever via a 20× objective lens (CFI S Plan Fluor ELWD, Nikon). Dynamic alteration of the laser position due to cantilever deflection was captured by a position-sensing two-segmented photodiode. The structural integrity of the HA0 trimer was protected by setting the free oscillation amplitude of the cantilever ($A_0$) to 1.5–2.5 nm and the set point to 80%–90% of the free amplitude to achieve a small tip-sample loading force.

### 2.4. Analysis of HS-AFM images

HS-AFM images were processed and analyzed using ImageJ software (imagej.nih.gov/ij/). First, x and y directions of images were filtered by a fit polynomial filter followed by a Gaussian blur filter (Sigma:1) to reduce noise. Several parameters of HA0 trimers such as length, width, and height were measured using ImageJ. Both Fast Fourier Transformation (FFT) and circularity measurement were performed using the plugin functions available in ImageJ software. FFT was performed by choosing the FFT bandpass filter function and then pixel filtration for both large and small structures were adjusted to obtain good resolution images. A circularity value of 1.0 indicates a perfect circle. As the value approaches 0.0, it indicates an increasingly elongated polygon. The circularity of the HA0 is defined by $4\pi S L^{-2}$, where L and S are its perimeter and the area surrounded by the HA0. The volume of HA0 was calculated by multiplying the area and height as mentioned previously [36].

### 2.5. Statistical analysis

Statistical analysis was conducted using SPSS version 22 (IBM Corp). Comparisons of continuous variables (area, circularity, height, and volume) between $HA0_{neutral}$ and $HA0_{acid}$ were using the Mann–Whitney $U$ test. The statistical significance level was set at $p < .05$ with a confidence interval of 95%.

## 3. Results and discussion

### 3.1. Direct visualization of the trimeric hemagglutinin precursor (HA0) of H5N1 using high-speed atomic force microscopy (HS-AFM)

The protein structure of the recombinant HA of H5N1 with uncleaved HA1 and HA2 domains, also is known as the HA precursor (HA0), was investigated using HS-AFM. To probe the potential heterogeneity and dynamics of HA0 at nanoscale, we employed a laboratory-built high-speed atomic force microscope mounted on an inverted microscope (Fig. 1A). There are three different modes available for image acquisition in AFM [37], known as the contact, tapping, and jumping modes. HS-AFM adopts the so-called amplitude modulation or 'tapping-mode' [38], in which the tip is upright oscillated at the first resonant frequency of the cantilever and occasionally contacts the sample surface throughout raster scanning. The amplitude modulation mode is functional for delicate and soft substrate-adsorbed biological samples, since the sporadic and irregular contact between the tip and sample significantly decreases the lateral friction force during scanning and consequently minimizes damage and deformation of protein molecules [39]. The cantilever oscillation amplitude is sensed by an optical-beam-defection technique and kept constant to a reference amplitude by a proportional-integral-derivative (PID) feedback controller that drives the z-piezo to compensate for tip-sample separation distance changes, subsequently keeping the interaction force between the tip and sample constant [39]. Then the AFM topographic image is built by recording the PID signal (z-dimension) at each pixel (x,y-dimensions) (Fig. 1A). During scanning, recombinant HA0 trimers were loaded on a flat muscovite mica layer coated on a glass stage mounted on a HS-AFM scanner as demonstrated in Fig. 1A.

Before performing the HS-AFM experiments, we first studied the HA

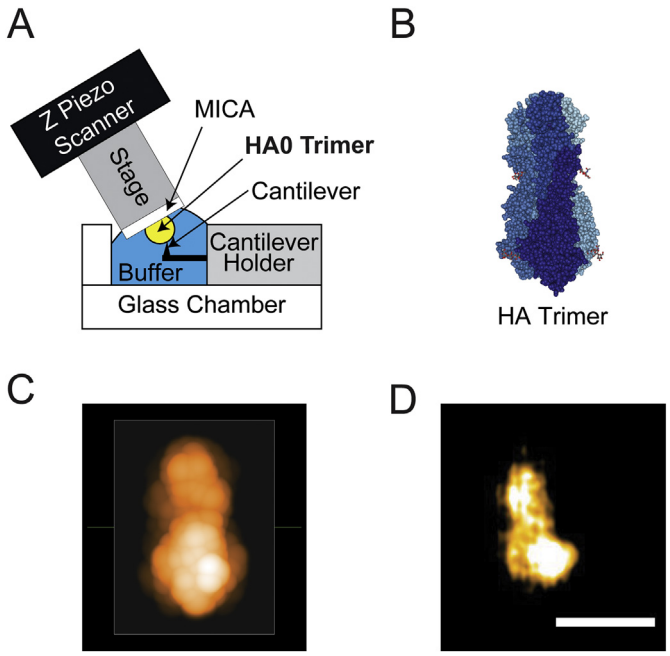


**Fig. 1.** HS-AFM setup for direct visualization of HA0 trimer. A) Schematic diagram of the HS-AFM setup for scanning the HA0 trimer. B) Crystal structure of HA trimer of H5N1 (PDB code: 2FK0). C) Simulated AFM image of HA trimer of H5N1 derived from 2FK0. D) Real-time image of HA0 trimer treated with 4% PFA in 50 mM Tris-HCl (pH: 7.4) captured by HS-AFM. Fast Fourier transformation (FFT) was applied with a maximum of 60 pixels for large structures and a minimum of 3 pixels for smaller structures (tolerance: 5%). Scale bar: 15 nm.

trimer structure based on information available from the RCSB protein data bank website (https://www.rcsb.org/). We found that the molecular structures and dimensions of the HA0 trimer (PDB code: 1HA0) and HA trimer (PDB code: 4FNK) of H3N2 were comparable suggesting that cleavage of HA0 trimer by proteases does not change the trimeric structure of the HA (supplementary Fig. S1). Therefore, the HA trimer of H5N1 (2FK0) is a suitable reference to study the HA0 trimer of H5N1 (Fig. 1B). Furthermore, each monomer of HA0 consists of about 568 amino acids (GenBank accession number: AAC32099.1) and each monomer assembles to form a noncovalent trimer [40]. We combined this information to generate an AFM simulation image using HS-AFM simulation software (SPM simulator, Advanced Algorithm Systems). Using a virtual scanning probe as described in a previous study [41], a simulated image of HA0 trimer was obtained, as shown in Fig. 1C. Next, we scanned the structure of 4% paraformaldehyde (PFA)-fixed HA0 trimer using HS-AFM. Conventional imaging tools for protein structural studies such as cryo-EM require sample fixation. Nevertheless, sample fixation is not compulsory for HS-AFM imaging. We only performed PFA fixation for getting PFA-fixed HA0 images and we used native HA0 proteins for the rest of our experiments. We suggest that PFA fixation increases rigidity of HA0 and this could help us to obtain HA0 images scanned by HS-AFM as resemble as possible to the images observed in conventional imaging tools. According to our results, the structure of PFA-fixed HA0 trimer in HS-AFM was almost similar to the simulated image constructed from the crystal structure of 2FK0 (Fig. 1D). The lower part of HA0 was globular, suggesting the globular head, and the upper part of HA0 was slimmer, suggesting the stalk domain.

Next, we monitored HA0s coated on mica under HS-AFM. We successfully captured real-time images of $HA0_{neutral}$ at a speed of 5 fps (Fig. 2A; Supplementary Movie 1). Although HS-AFM showed that HA0 trimer remains in elongated shape under physiological buffer, when we compared with the PFA-fixed HA0 trimer, we found that the globular head domain and stalk domain were less noticeable. This finding could

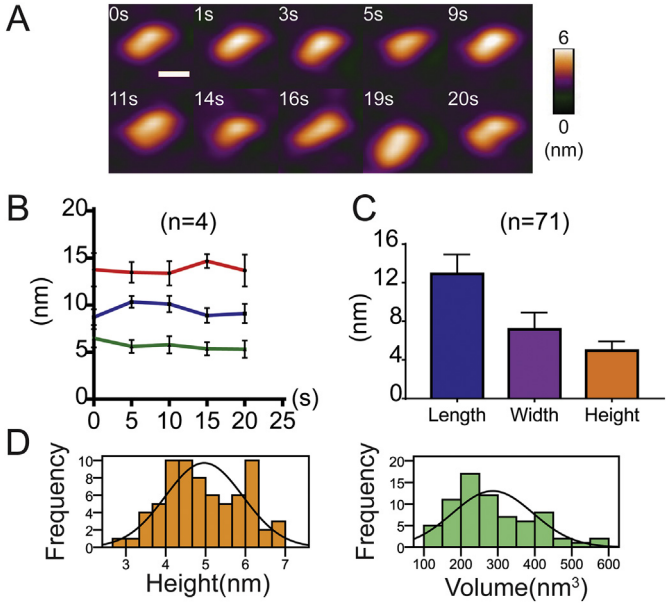


**Fig. 2.** Structural dynamics of HA0 of H5N1 under neutral conditions (pH:7.4). A) Real-time images of HA0 in 50 mM Tris-HCl (pH:7.4) captured by HS-AFM at 5 fps. Scale bar, 15 nm B) Dynamic changes in the length (red), width (blue), and height (green) of HA0 (s: seconds). C) Average length, width, and height of HA0 molecules ($n$ = 71). Data are shown as mean ± SD. D) Distribution of the height and volume of HA0 under neutral conditions are depicted in histograms with a normal distribution curve.

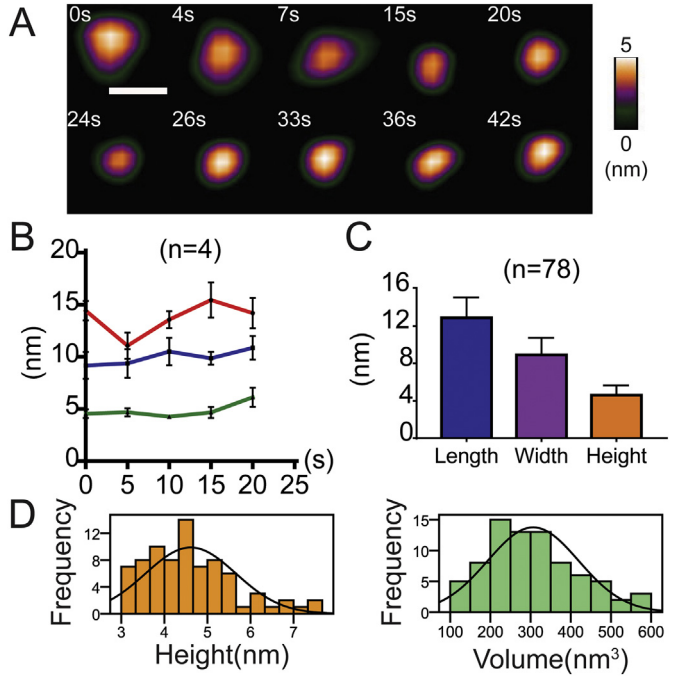


**Fig. 3.** Structural dynamics of HA0 of H5N1 under acidic conditions (pH: 5.0). A) Real-time images of HA0 in 50 mM Tris-HCl titrated with acetic acid (pH: 5.0) captured by HS-AFM at 5 fps. Scale bar, 15 nm. B) Dynamic changes in the length (red), width (blue), and height (green) of HA0 (s: seconds). C) Average length, width, and height of HA0 molecules ($n$ = 78). Data are shown as the mean ± SD. D) Distribution of the height and volume of HA0 under acidic conditions are illustrated in histograms with a normal curve.

**Table 1**
Dimensions of HA measured from PDB files.

| Trimeric hemagglutinin | Length (nm) | Width (nm) | Height (nm) |
|---|---|---|---|
| HA0 H3N2 (PDB: 1HA0) | 13.5 | 6.9 | 6.9 |
| HA H3N2 (PDB: 4FNK) | 13.4 | 6.4 | 6 |
| HA H5N1 (PDB: 2FK0) | 13.5 | 6.3 | 6.9 |

reflect the nature behavior of HA0 trimer folding in physiological buffer. HA0 trimers were adsorbed onto a mica surface in lateral orientation due to the high surface area. We meticulously performed image processing and analysis to minimize the catastrophic effect of noise on sample measurement. The dynamic changes in length, width, and height of the HA0 trimer ($n$ = 4) were measured (Fig. 2B). The average length, width, and height measured from 71 HA0 trimers were 12.91 nm, 7.17 nm, and 4.96 nm respectively (Fig. 2C and Table 2). Histograms with Gaussian curves for both height and volume are shown in Fig. 2D. According to our results (Table 2), the dimensions of HA0 trimer in Tris buffer were comparable to the dimensions of several HA measured from the PDB files (Table 1). The small discrepancies in measurement of HA0 trimer between X-ray crystallography and HS-AFM could be due to type of sample (protein crystal versus native protein), adsorption effect of mica [29], or the interaction between cantilever and protein samples.

We noted that the tapping mode, also known as the intermittent contact mode in HS-AFM, allows the scanning probe to contact the HA0 trimer at a fast pace (from subsecond to sub-100-ms speed) avoiding the friction force experienced during lateral scanning [42], thereby protecting the integrity of the HA0 trimer. Moreover, our results were comparable to those published by Barinov and coworkers [29] who used high-resolution AFM to observe the HAs of various subtypes of influenza A. According to their findings, the volume of HA of H5N1 were mostly in the range of 100 to 300 $nm^3$ in which was comparable to our results (150 to 450 $nm^3$; Fig. 2D). By contrast, the height of trimeric HA measured by high-resolution AFM (2 .5nm) was far lesser than the height of trimeric HA measured by X-ray crystallography (Table 1). This difference may suggest that the scanning force of HS-AFM on HA0 trimer is much lower than that in high-resolution AFM [29]. As a result, HS-AFM not only could provide direct visualization of the dynamics of HA0 trimers, as suggested by previous structural studies [7,13,14,17] and FRET experiments [21] but also much more precise in protein measurement when compared with high-resolution AFM.

### 3.2. Low pH induces conformational changes in HA0 trimer

In previous studies, several indirect approaches have been used to determine acid-induced irreversible conformational changes in HA proteins. For example, by evaluating the susceptibility of HA to trypsin digestion [43], by detecting antigens in HA using a panel of conformational specific monoclonal antibodies [5,44], or by detecting the acquisition of hydrophobic properties in the hydrophilic domain [43]. Boulay and colleagues performed a trypsin susceptibility test and immunoprecipitation to investigate the conformation of HA0 trimers under low pH conditions [19]. They found that HA0 trimer underwent an irreversible conformational change after exposure to acidic condition for 30 min; however, the acid-induced conformation of HA0 trimer was fusogenic incompetent. Seven years later, using x-ray crystallography, Bullough and coworkers reported that HA0 trimer was stable under acidic conditions. However, HA trimer was metastable under acidic conditions and undergoes a rapid irreversible conformational change in endosomes to induce membrane fusion [20]. To answer the ambiguous conformation properties of HA0 trimer in acidic conditions, we set out to visualize and analyze the structural changes of HA0 trimer under acidic conditions using HS-AFM. The dynamic structure of $HA0_{acid}$ trimer is shown in Fig. 3A (also Supplementary Movie 2). The dynamic changes in length, width, and height of the HA0 trimer ($n$ = 4) were measured (Fig. 3B). Like $HA0_{neutral}$, we found that the fluctuations in length and width of $HA0_{acid}$ were much higher than the fluctuations

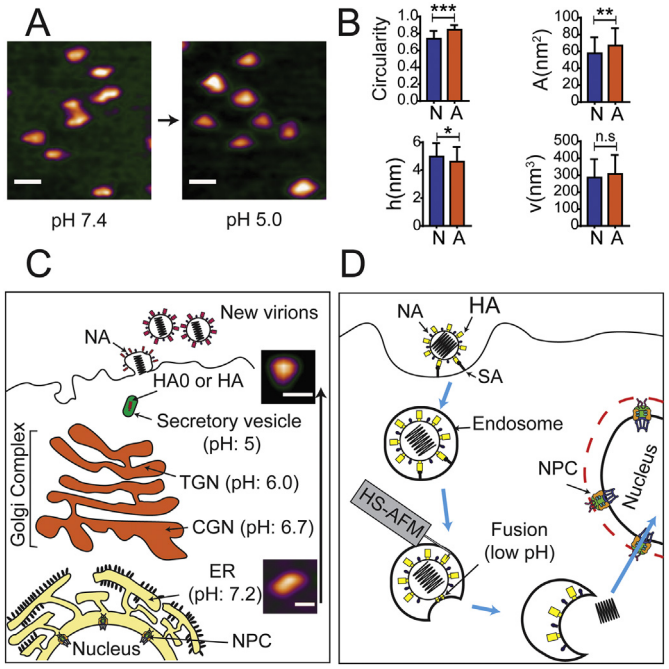


**Fig. 4.** Low pH environment induces conformational change of HA0. A) HA0 shows different conformations in neutral and acidic environments. Scale bar, 25 nm. B) Comparisons of circularity, area(A), height(h) and volume(v) between HA0 in neutral pH (N; n = 71) and HA0 in acidic pH (A; n = 78). Data are demonstrated as mean ± SD. *p* values were computed by Mann-Whitney *U* test (* $p < .05$; ** $p < .01$, *** $p < .001$). C) Conformational change of HA0 trimer in neutral and acidic condition mimics to the pH gradient from ER to secretory vesicles during viral assembly in cell membrane (ER: endoplasmic reticulum; CGN: *cis*-Golgi network; TGN: *trans*-Golgi network; NPC: nuclear pore complex). D) Strategy for direct visualization of complex and highly dynamic HA structure during viral entry in near future (HA: hemagglutinin, NA: neuraminidase, NPC: nuclear pore complex).

in height. There is no significant different in magnitude of fluctuation of these parameters between $HA0_{neutral}$ and $HA0_{acid}$ (Supplementary Fig. S2). We also measured the average dimensions of $HA0_{acid}$ ($n = 78$), which were 12.89nm (length), 8.92 nm (width), and 4.61 nm (height) (Fig. 3C and Table 2). The distribution of height and volume of $HA0_{acid}$ are presented in histograms together with Gaussian's curve in Fig. 3D.

By comparing the morphology of $HA0_{neutral}$ with $HA0_{acid}$, we noticed that HA0 underwent expansion under acidic conditions (Fig. 4A and Supplementary Movie 3). There is a possibility that the HS-AFM tip interaction and image drift might be involved, but this seems unlikely because the circular form populates the same movie frames (Fig. 4A). We measured the height and volume of $HA0_{acid}$ and asserted that the trimeric structure was retained under acidic conditions because we hardly detected any small-sized particles, including HA monomers in our experiments. To compare the conformational changes in HA0 trimer induced by low pH conditions, we processed the HS-AFM images using ImageJ software to analyze the quantitative data for various parameters such as area, circularity, height and volume. The circularity of the HA0 trimer was included for comparison because $HA0_{acid}$ appeared more circular than $HA0_{neutral}$ (Fig. 4A). Statistical analysis showed that low pH significantly increased the area ($p < .01$) and circularity ($p < .001$) of HA0 trimer, and significantly reduced the height ($p < .05$) (Fig. 4B). The reduction of height could offset the change of volume as the volume of $HA0_{neutral}$ was comparable to the volume of $HA0_{acid}$. Our results indicate that HA0 trimers could undergo expansion in acidic condition as reported by Boulay and coworkers about the sensitivity of HA0 trimer to acidic conditions. Acid-induced longitudinal ectodomain torsion follow by dilation of the central cavity in the HA trimer are important functional motions to release fusion peptide in endosomes [45,46]. These mechanical activities and could explain the expansion of $HA0_{acid}$. However, the dynamics could be restricted by peptide chains in the cleavage site and therefore remain fusogenic incompetent.

HA monomers are synthesized and trimerized as HA0 trimers in the ER before translocate to the Golgi complex [47]. Avian influenza A subtypes 5 and 7 belong to the highly pathogenic avian influenza (HPAI) viruses in which the HA contains a polybasic cleavage site with the sequence RRRKKR↓G (down arrow indicates the cleavage site) [48,49]. The sequence is recognized by a subtilisin-like endoprotease known as furin [50]. Cleavage of HA0 trimers of subtypes 5 and 7 occurs in the *trans*-Golgi network (TGN), the main localization site of furin [51]. By contrast, HA0 trimers of low pathogenic avian influenza (LPAI) are cleaved by extracellular proteases such as HAT and TMPPRS2 [8]. Similarly, our recombinant HA0 trimer possessed a mutated cleavage site (RRRKKR-TETR) and therefore can be cleaved by trypsin but not furin [52]. HA0 trimers or HA trimers are transported from the TGN to the cell membrane in clear secretory vesicles for viral assembly [53]. From the ER to the secretory vesicle, the pH level in the compartments descends as shown in Fig. 4C. Our findings on the structural dynamics between $HA0_{neutral}$ and $HA0_{acid}$ therefore mimics the conformation of HA0 trimers of LPAI when the trimers are translocated from the ER to secretory vesicles ($pH_{ER}$: 7.2 to $pH_{secretory\ vesicles}$: 5) [54,55]. Das and colleagues reported comprehensively on the reversibility of the conformational dynamics of HA trimer after a short period of exposure (< 30 min) to acidic conditions [21]. According to Boulay and colleagues, an irreversible conformational change in HA0 trimer was found after incubation in acidic conditions for 30 min [19]. To investigate the reversibility of HA0 trimer from acidic to neutral condition, we conducted our experiment in this arrangement: pH 7.4-pH 5-pH 7.4 (Supplementary Movie 4). Same sample was loaded on mica and scanned continuously throughout this experiment. HA0 trimer was exposed to acidic Tris buffer for 20 min before the sample was neutralized to pH 7.4. The major challenge in this experiment was inability to scan similar region as we need to lift up the scanner and changed the medium with different pH. Collectively, by scanning on different regions, we did observe the expansion of HA0 trimer in acidic condition. Interestingly, we did observe HA0 trimer structure was partially reversible after the pH had been neutralized to 7.4 (Supplementary Movie 4). This finding indeed is exhilarating yet our current setting is still not ideal to illustrate the complete conformational transition of HA0 trimers between neutral and acidic conditions. We suggest that additional optimizations or improvement of HS-AFM instrumental design are needed to overcome above mentioned challenges to achieve this goal in future study.

Using HS-AFM, biological events can be visualized in a way that may not be possible using other approaches. The ambiguity of the

**Table 2**
Physical properties of HA0 in both neutral and acidic conditions measured by using HS-AFM.

| Trimeric hemagglutinin | Mean ± SD | | | | | |
|---|---|---|---|---|---|---|
| | Length (nm) | Width (nm) | Height (nm) | Area ($nm^2$) | Volume ($nm^3$) | Circularity |
| $HA0_{neutral}$ (n = 71) | 12.91 ± 2.02 | 7.17 ± 1.75 | 4.96 ± 0.97 | 57.64 ± 19.07 | 286.41 ± 108.84 | 0.74 ± 0.09 |
| $HA0_{acid}$ (*n* = 78) | 12.89 ± 2.18 | 8.92 ± 1.82 | 4.61 ± 1.05 | 66.80 ± 20.65 | 306.43 ± 113.06 | 0.84 ± 0.06 |

$HA0_{acid}$ conformation is a good example of this. Understanding the life cycle (Fig. 4D) and dynamic structure of HA is essential for determining an effective therapeutic strategy against H5N1. Compared with HA0 trimer, the structural dynamics of the HA trimer, particularly the HA2 domain, are much more dynamic and complex. To date, the complex and reversible structural dynamics of HA under acidic conditions have only been analyzed using FRET. Besides HA, the nuclear export protein NS2 of influenza A is also a potential target for antiviral drugs. NS2 contains a leucine-rich nuclear-export signal that could guide viral ribonucleoproteins to cross the nuclear pore complex [56–59], thereby interacting with Nup98 and undergoing directional nucleocytoplasmic trafficking [60] (Fig. 4D). We strongly believe that HS-AFM is an ideal tool with which to capture and decipher images of the spatiotemporal dynamic structures of influenza proteins such as HA2 and NS2 in the future.

### 3.3. Conclusion

In conclusion, we report for the first time the real-time conformational behavior of HA0 trimer of H5N1 in liquid using HS-AFM. We have provided direct and compelling evidences to show that HA0 trimers undergo expansion in acidic environment. Although we manage to demonstrate the reversibility of conformational changes of HA0 trimer after neutralization, further study is needed to confirm this phenomenon. It is sensible to hypothesize that HA0 trimer has structural reversibility otherwise LPAI virions should not be infectious as HA0 trimers experience irreversible conformational changes in acidic TGN or secretory granules. Our work establishes HS-AFM as an inimitable tool to directly study viral protein dynamics, which are difficult to capture with low signal-to-noise techniques relying on ensemble averaging, such as cyro-EM and X-ray crystallography. With high scanning speed and a minimally invasive cantilever, we predict that HS-AFM is feasible to reveal the flow of irreversible conformational changes of HA2 induced by low pH, which is mimicking the true biological events that occur when HA enters a host endosome, in future study.

Supplementary data to this article can be found online at https://doi.org/10.1016/j.bbagen.2019.02.015.

## Acknowledgements

We thank Gunter Blobel (1936–2018), a passionate cell biologist and inspirational mentor for helpful discussions. We also thank all members of the Wong laboratory. This work was supported by a WPI NanoLSI start-up fund (to K.L.); MEXT/JSPS KAKENHI grant numbers 17H05874 and 17K08655 (to R.W.) from MEXT Japan, and by grants from the Kobayashi International Scholarship Foundation (to R.W), and the Shimadzu Science Foundation (to R.W.).

## References

[1] T. Horimoto, T. Kawaoka, Influenza: lessons from past pandemics, warnings from current incidents, Nat. Rev. Microbiol. 3 (2005) 591–600, https://doi.org/10.1038/nrmicro1208.
[2] M. Wang, M. Veit, Hemagglutinin-esterase-fusion (HEF) protein of influenza C virus, Protein Cell 7 (2016) 28–45, https://doi.org/10.1007/s13238-015-0193-x.
[3] P. Palese, Influenza: old and new threats, Nat. Med. 10 (2004) S82–S87, https://doi.org/10.1038/nm1141.
[4] S.E. Lindstrom, N.J. Cox, A. Klimov, Genetic analysis of human H2N2 and early H3N2 influenza viruses, 1957–1972: evidence for genetic divergence and multiple reassortment events, Virology 328 (2004) 101–119, https://doi.org/10.1016/j.virol.2004.06.009.
[5] C.S. Copeland, R.W. Doms, E.M. Bolzau, R.G. Webster, A. Helenius, Assembly of influenza hemagglutinin trimers and its role in intracellular transport, J. Cell Biol. 103 (1986) 1179–1191.
[6] C.M. Mair, K. Ludwig, A. Herrmann, C. Sieben, Receptor binding and pH stability - how influenza A virus hemagglutinin affects host-specific virus infection, Biochim. Biophys. Acta 1838 (2014) 1153–1168, https://doi.org/10.1016/j.bbamem.2013.10.004.
[7] J. Chen, K.H. Lee, D.A. Steinhauer, D.J. Stevens, J.J. Skehel, D.C. Wiley, Structure of the hemagglutinin precursor cleavage site, a determinant of influenza pathogenicity and the origin of the labile conformation, Cell. 95 (1998) 409–417.
[8] E. Böttcher, T. Matrosovich, M. Beyerle, H.D. Klenk, W. Garten, M. Matrosovich, Proteolytic activation of influenza viruses by serine proteases TMPRSS2 and HAT from human airway epithelium, J. Virol. 80 (2006) 9896–9898, https://doi.org/10.1128/JVI.01118-06.
[9] G.N. Rogers, J.C. Paulson, Receptor determinants of human and animal influenza virus isolates: differences in receptor specificity of the H3 hemagglutinin based on species of origin, Virology. 127 (1983) 361–373.
[10] A.S. Gambaryan, J.S. Robertson, M.N. Matrosovich, Effects of egg-adaptation on the receptor-binding properties of human influenza A and B viruses, Virology 258 (1999) 232–239, https://doi.org/10.1006/viro.1999.9732.
[11] A.S. Gambaryan, T.Y. Matrosovich, J. Philipp, V.J. Munster, R.A. Fouchier, G. Cattoli, I. Capua, S.L. Krauss, R.G. Webster, J. Banks, N.V. Bovin, H.D. Klenk, M.N. Matrosovich, Receptor-binding profiles of H7 subtype influenza viruses in different host species, J. Virol. 86 (2012) 4370–4379, https://doi.org/10.1128/JVI.06959-11.
[12] M.N. Matrosovich, A.S. Gambaryan, S. Teneberg, V.E. Piskarev, S.S. Yamnikova, D.K. Lvov, J.S. Robertson, K.A. Karlsson, Avian influenza A viruses differ from human viruses by recognition of sialyloligosaccharides and gangliosides and by a higher conservation of the HA receptor-binding site, Virology 233 (1997) 224–234, https://doi.org/10.1006/viro.1997.8580.
[13] J. Stevens, O. Blixt, T.M. Tumpey, J.K. Taubenberger, J.C. Paulson, I.A. Wilson, Structure and receptor specificity of the hemagglutinin from an H5N1 influenza virus, Science 312 (2006) 404–410, https://doi.org/10.1126/science.1124513.
[14] D.J. Benton, A. Nans, L.J. Calder, J. Turner, U. Neu, Y.P. Lin, E. Ketelaars, N.L. Kallewaard, D. Corti, A. Lanzavecchia, S.J. Gamblin, P.B. Rosenthal, J.J. Skehel, Influenza hemagglutinin membrane anchor, Proc. Natl. Acad. Sci. U. S. A. 115 (2018) 10112–10117, https://doi.org/10.1073/pnas.1810927115.
[15] K.E. Gallagher, D.S. LaMontagne, D. Watson-Jones, Status of HPV vaccine introduction and barriers to country uptake, Vaccine 36 (2018) 4761–4767, https://doi.org/10.1016/j.vaccine.2018.02.003.
[16] V. Moules, O. Terrier, M. Yver, B. Riteau, C. Moriscot, O. Ferraris, T. Julien, E. Giudice, J.P. Rolland, A. Erny, M. Bouscambert-Duchamp, E. Frobert, M. Rosa-Calatrava, Y. Pu Lin, A. Hay, D. Thomas, G. Schoehn, B. Lina, Importance of viral genomic composition in modulating glycoprotein content on the surface of influenza virus particles, Virology 414 (2011) 51–62, https://doi.org/10.1016/j.virol.2011.03.011.
[17] C. McCullough, M. Wang, L. Rong, M. Caffrey, Characterization of influenza hemagglutinin interactions with receptor by NMR, PLoS One 7 (2012) e33958, , https://doi.org/10.1371/journal.pone.0033958.
[18] S. Elli, E. Macchi, T.R. Rudd, R. Raman, G. Sassaki, K. Viswanathan, E.A. Yates, Z. Shriver, A. Naggi, G. Torri, R. Sasisekharan, M. Guerrini, Insights into the human glycan receptor conformation of 1918 pandemic hemagglutinin-glycan complexes derived from nuclear magnetic resonance and molecular dynamics studies, Biochemistry. 53 (2014) 4122–4135, https://doi.org/10.1021/bi500338r.
[19] F. Boulay, R.W. Doms, I. Wilson, A. Helenius, The influenza hemagglutinin precursor as an acid-sensitive probe of the biosynthetic pathway, EMBO J. 6 (1987) 2643–2650.
[20] P.A. Bullough, F.M. Hughson, J.J. Skehel, D.C. Wiley, Structure of influenza haemagglutinin at the pH of membrane fusion, Nature 371 (1994) 37–43, https://doi.org/10.1038/371037a0.
[21] D.K. Das, R. Govindan, I. Nikić-Spiegel, F. Krammer, E.A. Lemke, J.B. Munro, Direct visualization of the conformational dynamics of single influenza hemagglutinin trimers, Cell 174 (2018) 926–937 e12 https://doi.org/10.1016/j.cell.2018.05.050.
[22] P. Hinterdorfer, Y.F. Dufrene, Detection and localization of single molecular recognition events using atomic force microscopy, Nat. Methods 3 (2006) 347–355, https://doi.org/10.1038/nmeth871.
[23] C. Stroh, H. Wang, R. Bash, B. Ashcroft, J. Nelson, H. Gruber, D. Lohr, S.M. Lindsay, P. Hinterdorfer, Single-molecule recognition imaging microscopy, Proc. Natl. Acad. Sci. U. S. A. 101 (2004) 12503–12507, https://doi.org/10.1073/pnas.0403538101.
[24] J.M. Fernandez, H. Li, Force-clamp spectroscopy monitors the folding trajectory of a single protein, Science 303 (2004) 1674–1678, https://doi.org/10.1126/science.1092497.
[25] P.M. Williams, S.B. Fowler, R.B. Best, J.L. Toca-Herrera, K.A. Scott, A. Steward, J. Clarke, Hidden complexity in the mechanical properties of titin, Nature 422 (2003) 446–449, https://doi.org/10.1038/nature01517.
[26] A. Touhami, B. Nysten, Y.F. Dufrêne, Nanoscale mapping of the elasticity of microbial cells by atomic force microscopy, Langmuir 19 (2003) 4539–4543, https://doi.org/10.1021/la034136x.
[27] T. Fukuma, Y. Okazaki, N. Kodera, T. Uchihashi, T. Ando, High resonance frequency force microscope scanner using inertia balance support, Appl. Phys. Lett. 92 (2008), https://doi.org/10.1063/1.2951594.
[28] M.P. Stewart, J. Helenius, Y. Toyoda, S.P. Ramanathan, D.J. Muller, A.A. Hyman, Hydrostatic pressure and the actomyosin cortex drive mitotic cell rounding, Nature 469 (2011) 226–230, https://doi.org/10.1038/nature09642.
[29] N. Barinov, N. Ivanov, A. Kopylov, D. Klinov, E. Zavyalova, Direct visualization of the oligomeric state of hemagglutinins of influenza virus by high-resolution atomic force microscopy, Biochimie 146 (2018) 148–155, https://doi.org/10.1016/j.biochi.2017.12.014.
[30] T. Ando, T. Uchihashi, T. Fukuma, High-speed atomic force microscopy for nano-visualization of dynamic biomolecular processes, Prog. Surf. Sci. 83 (2008) 337–437, https://doi.org/10.1016/j.progsurf.2008.09.001.
[31] N. Kodera, D. Yamamoto, R. Ishikawa, T. Ando, Video imaging of walking myosin V by high-speed atomic force microscopy, Nature 468 (2010) 72–76, https://doi.org/10.1038/nature09450.
[32] M. Shibata, H. Nishimasu, N. Kodera, S. Hirano, T. Ando, T. Uchihashi, O. Nureki,

Real-space and real-time dynamics of CRISPR-Cas9 visualized by high-speed atomic force microscopy, Nat. Commun. 8 (2017) 1430, https://doi.org/10.1038/s41467-017-01466-8.
[33] T. Mori, S. Sugiyama, M. Byrne, C.H. Johnson, T. Uchihashi, T. Ando, Revealing circadian mechanisms of integration and resilience by visualizing clock proteins working in real time, Nat. Commun. 9 (2018) 3245, https://doi.org/10.1038/s41467-018-05438-4.
[34] M.S. Mohamed, A. Kobayashi, A. Taoka, T. Watanabe-Nakayama, Y. Kikuchi, M. Hazawa, T. Minamoto, Y. Fukumori, N. Kodera, T. Uchihashi, T. Ando, R.W. Wong, High-speed atomic force microscopy reveals loss of nuclear pore resilience as a dying code in colorectal cancer cells, ACS Nano 11 (2017) 5567–5578, https://doi.org/10.1021/acsnano.7b00906.
[35] Y. Ruan, K. Kao, S. Lefebvre, A. Marchesi, P.J. Corringer, R.K. Hite, S. Scheuring, Structural titration of receptor ion channel GLIC gating by HS-AFM, Proc. Natl. Acad. Sci. U. S. A. 115 (2018) 10333–10338, https://doi.org/10.1073/pnas.1805621115.
[36] M.E. Fuentes-Perez, M.S. Dillingham, F. Moreno-Herrero, AFM volumetric methods for the characterization of proteins and nucleic acids, Methods. 60 (2013) 113–121, https://doi.org/10.1016/j.ymeth.2013.02.005.
[37] F. Moreno-Herrero, J. Colchero, J. Gómez-Herrero, A.M. Baró, Atomic force microscopy contact, tapping, and jumping modes for imaging biological samples in liquids, Phys. Rev. E Stat. Nonlinear Soft Matter Phys. 69 (2004) 031915, , https://doi.org/10.1103/PhysRevE.69.031915.
[38] P.K. Hansma, J.P. Cleveland, M. Radmacher, D.A. Walters, P.E. Hillner, M. Bezanilla, M. Fritz, D. Vie, H.G. Hansma, Tapping mode atomic force microscopy in liquids, Appl. Phys. Lett. 64 (1994) 1738–1740, https://doi.org/10.1063/1.111795.
[39] T. Uchihashi, S. Scheuring, Applications of high-speed atomic force microscopy to real-time visualization of dynamic biomolecular processes, Biochim. Biophys. Acta Gen. Subj. 1862 (2018) 229–240, https://doi.org/10.1016/j.bbagen.2017.07.010.
[40] P.S. Lee, X. Zhu, W. Yu, I.A. Wilson, Design and structure of an engineered disulfide-stabilized influenza virus hemagglutinin trimer, J. Virol. 89 (2015) 7417, https://doi.org/10.1128/JVI.00808-15.
[41] T. Uchihashi, R. Iino, T. Ando, H. Noji, High-speed atomic force microscopy reveals rotary catalysis of rotorless F(1)-ATPase, Science 333 (2011) 755–758, https://doi.org/10.1126/science.1205510.
[42] T. Ando, T. Uchihashi, N. Kodera, High-speed AFM and applications to biomolecular systems, Annu. Rev. Biophys. 42 (2013) 393–414, https://doi.org/10.1146/annurev-biophys-083012-130324.
[43] J.J. Skehel, P.M. Bayley, E.B. Brown, S.R. Martin, M.D. Waterfield, J.M. White, I.A. Wilson, D.C. Wiley, Changes in the conformation of influenza virus hemagglutinin at the pH optimum of virus-mediated membrane fusion, Proc. Natl. Acad. Sci. U. S. A. 79 (1982) 968–972.
[44] R.G. Webster, L.E. Brown, D.C. Jackson, Changes in the antigenicity of the hemagglutinin molecule of H3 influenza virus at acidic pH, Virology. 126 (1983) 587–599.
[45] C. Böttcher, K. Ludwig, A. Herrmann, M. van Heel, H. Stark, Structure of influenza haemagglutinin at neutral and at fusogenic pH by electron cryo-microscopy, FEBS Lett. 463 (1999) 255–259.
[46] B. Isin, P. Doruker, I. Bahar, Functional motions of influenza virus hemagglutinin: a structure-based analytical approach, Biophys. J. 82 (2002) 569–581, https://doi.org/10.1016/S0006-3495(02)75422-2.
[47] C.S. Copeland, K.P. Zimmer, K.R. Wagner, G.A. Healey, I. Mellman, A. Helenius, Folding, trimerization, and transport are sequential events in the biogenesis of influenza virus hemagglutinin, Cell. 53 (1988) 197–209 (s).
[48] V.J. Munster, E.J. Schrauwen, E. de Wit, J.M. van den Brand, T.M. Bestebroer, S. Herfst, G.F. Rimmelzwaan, A.D. Osterhaus, R.A. Fouchier, Insertion of a multibasic cleavage motif into the hemagglutinin of a low-pathogenic avian influenza H6N1 virus induces a highly pathogenic phenotype, J. Virol. 84 (2010) 7953–7960, https://doi.org/10.1128/JVI.00449-10.
[49] M.A. Izidoro, I.E. Gouvea, J.A. Santos, D.M. Assis, V. Oliveira, W.A. Judice, M.A. Juliano, I. Lindberg, L. Juliano, A study of human furin specificity using synthetic peptides derived from natural substrates, and effects of potassium ions, Arch. Biochem. Biophys. 487 (2009) 105–114, https://doi.org/10.1016/j.abb.2009.05.013.
[50] A. Stieneke-Grober, M. Vey, H. Angliker, E. Shaw, G. Thomas, C. Roberts, H.D. Klenk, W. Garten, Influenza virus hemagglutinin with multibasic cleavage site is activated by furin, a subtilisin-like endoprotease, EMBO J. 11 (1992) 2407–2414.
[51] S. Takahashi, T. Nakagawa, T. Banno, T. Watanabe, K. Murakami, K. Nakayama, Localization of furin to the trans-Golgi network and recycling from the cell surface involves Ser and Tyr residues within the cytoplasmic domain, J. Biol. Chem. 270 (1995) 28397–28401.
[52] S.M. Kang, D.G. Yoo, A.S. Lipatov, J.M. Song, C.T. Davis, F.S. Quan, L.M. Chen, R.O. Donis, R.W. Compans, Induction of long-term protective immune responses by influenza H5N1 virus-like particles, PLoS One 4 (2009) e4667, , https://doi.org/10.1371/journal.pone.0004667.
[53] L. Orci, M. Ravazzola, M. Amherdt, A. Perrelet, S.K. Powell, D.L. Quinn, H.P. Moore, The trans-most cisternae of the Golgi complex: a compartment for sorting of secretory and plasma membrane proteins, Cell 51 (1987) 1039–1051.
[54] A. Rivinoja, F.M. Pujol, A. Hassinen, S. Kellokumpu, Golgi pH, its regulation and roles in human disease, Ann. Med. 44 (2012) 542–554, https://doi.org/10.3109/07853890.2011.579150.
[55] M.M. Wu, J. Llopis, S. Adams, J.M. McCaffery, M.S. Kulomaa, T.E. Machen, H.P. Moore, R.Y. Tsien, Organelle pH studies using targeted avidin and fluorescein-biotin, Chem. Biol. 7 (2000) 197–209.
[56] T. Funasaka, V. Balan, A. Raz, R.W. Wong, Nucleoporin Nup98 mediates galectin-3 nuclear-cytoplasmic trafficking, Biochem. Biophys. Res. Commun. 434 (2013) 155–161, https://doi.org/10.1016/j.bbrc.2013.03.052.
[57] T. Funasaka, H. Nakano, Y. Wu, C. Hashizume, L. Gu, T. Nakamura, W. Wang, P. Zhou, M.A. Moore, H. Sato, R.W. Wong, RNA export factor RAE1 contributes to NUP98-HOXA9-mediated leukemogenesis, Cell Cycle 10 (2011) 1456–1467, https://doi.org/10.4161/cc.10.9.15494.
[58] K.S. Lim, R.W. Wong, Targeting nucleoporin POM121-importin beta axis in prostate cancer, Cell Chem. Biol. 25 (2018) 1056–1058, https://doi.org/10.1016/j.chembiol.2018.09.003.
[59] R.W. Wong, J.I. Mamede, T.J. Hope, Impact of nucleoporin-mediated chromatin localization and nuclear architecture on HIV integration site selection, J. Virol. 89 (2015) 9702–9705, https://doi.org/10.1128/JVI.01669-15.
[60] J. Chen, S. Huang, Z. Chen, Human cellular protein nucleoporin hNup98 interacts with influenza A virus NS2/nuclear export protein and overexpression of its GLFG repeat domain can inhibit virus propagation, J. Gen. Virol. 91 (2010) 2474–2484, https://doi.org/10.1099/vir.0.022681-0.